1562 *Biochemistry* **2006,** *45,* 1562−1570

Crystal Structure of Mouse Succinic Semialdehyde Reductase AKR7A5: Structural Basis for Substrate Specificity[†,‡]

Xiaofeng Zhu,[§,||] Adrian J. Lapthorn,*[,||] and Elizabeth M. Ellis[§]

Department of Chemistry, University of Glasgow, Glasgow G12 8QQ, U.K., and Departments of Bioscience and Pharmaceutical Sciences, University of Strathclyde, Glasgow G1 1XW, U.K.

Received August 12, 2005; Revised Manuscript Received November 3, 2005

ABSTRACT: The aldo-keto reductases make up a superfamily of enzymes which can reduce a variety of aldehydes and ketones to their corresponding alcohols. Within each family are distinct preferences for certain substrates, presumably reflecting their role within the cell. The original member of the AKR7A subfamily was purified from liver as an aflatoxin dialdehyde reductase AKR7A1. However, recent additions to the family have revealed that even closely related enzymes have clear substrate preferences with AKR7A2, AKR7A4, and AKR7A5 showing much higher affinities for succinic semialdehyde (SSA) than does AKR7A1. To investigate the structural basis of this specificity, the crystal structure of mouse AKR7A5 has been determined to better than 2.5 Å resolution. The structure is of the ternary complex of the enzyme with NADP$^+$ and tartrate as an inhibitor. This structure has the same overall fold as the previously determined structure of AKR7A1; however, there are a number of differences in loops around the active site that contribute to observed differences in the substrate specificity between the AKR7A enzymes. Several differences are the result of bulky hydrophobic residues found in AKR7A5, namely, Met44, Trp77, and Trp224, which significantly restrict the size and modify the architecture of the substrate-binding pocket, producing a tighter or less flexible binding site for SSA than in AKR7A1. Site-directed mutagenesis was used to introduce Met44, Trp77, and Trp224 individually into AKR7A1, to test if they improved the affinity of the enzyme for SSA. Each mutation showed improved affinity for SSA, with Trp77Met having the largest effect. This confirms the role of these amino acids as substrate determinants for SSA.

The aldo-keto reductases make up a superfamily of NAD(P)(H)-dependent oxidoreductases with broad physiological roles. These enzymes show considerable diversity in terms of substrate preference, each catalyzing the reduction of a range of aliphatic and aromatic aldehydes and ketones, including sugars, steroids, and xenobiotics. Most members of the superfamily are monomeric and share structural features, including a $(\beta/\alpha)_8$ barrel structure (*1*, *2*). The crystal structures of several members of the aldo-keto reductase family have now been determined (*3*−*8*), including that of the dimeric AKR7A1 (*9*, *10*), originally identified as rat liver aflatoxin dialdehyde reductase (*11*).

Four other members of the AKR7 family have now been cloned: human AKR7A2, human AKR7A3, rat AKR7A4, and mouse AKR7A5[1] (*12*−*15*). Their substrate specificities have been determined for a range of aldehyde and ketone substrates (*16*−*18*), and it is apparent that in addition to the detoxification of aflatoxin B1 dialdehyde, these enzymes are capable of contributing to the reduction of carbonyls in a range of physiological contexts. AKR7A2, AKR7A4, and AKR7A5 all have on average higher affinity for SSA than AKR7A1 (*12*, *14*, *15*), and there is mounting evidence to indicate that human AKR7A2 can function as a succinic semialdehyde (SSA) reductase in brain and may play a role in the synthesis of γ-hydroxybutyrate (GHB) (*19*).

On the basis of amino acid sequence similarities, the current AKR7A family members can be grouped into two separate subfamilies. This information, in conjunction with tissue distribution (*14*) and enzyme kinetic data (*12*, *15*), suggests that AKR7A2, AKR7A4, and AKR7A5 (group II) are functional orthologues, acting as SSA reductases, and that they differ in function from ARK7A1 (group I), which is proposed to play a role predominantly in detoxification (*11*).

In mouse, there appears to be only one AKR7A enzyme, AKR7A5, suggesting that mice lack the specific AKR7A detoxification enzyme. The occurrence of only one AKR7A gene is not unique to mouse: searching for AKR7A-related sequences in other completed eukaryotic genomes reveals that in lower vertebrate genomes, only one copy of a gene with significant sequence similarity can be found. In every case, this sequence encodes an enzyme that is more similar to AKR7A5 (group II) enzymes than AKR7A1 (group I)

[†] We are grateful for funding from the Universities of Glasgow and Strathclyde Synergy Fund. X.Z. is a recipient of an Overseas Research Scholarship Award.

[‡] The atomic coordinates and structure factors have been deposited in the Protein Data Bank as entries 2C91 and r2C91sf, respectively.

* To whom correspondence should be addressed: Department of Chemistry, University of Glasgow, Glasgow G12 8QQ, U.K. Telephone: +44 141-330 5940. Fax: +44 141-330 4888. E-mail: adrian@chem.gla.ac.uk.

[§] University of Strathclyde.

[||] University of Glasgow.

[1] Abbreviations: AKR7A5, mouse aldo-keto reductase/succinic semialdehyde reductase; AFB$_1$, aflatoxin B$_1$; 2-CBA, 2-carboxybenzaldehyde; DDT, dithiothreitol; GABA, γ-aminobutyric acid; GHB, γ-hydroxybutyric acid; NADP$^+$, oxidized form of nicotinamide adenine dinucleotide; SSA, succinic semialdehyde.

10.1021/bi051610k CCC: $33.50

enzymes. An understanding of the structural differences between AKR7A1 and AKR7A5 and their impact on substrate specificity may help explain species differences in aldehyde toxicity and metabolism among rat, mouse, and human and will provide a useful insight into the physiological roles of these enzymes *in vivo*.

We report here the crystal structure of AKR7A5 in complex with NADP$^+$ and tartrate. We have used the structure and site-directed mutagenesis to examine the basis for the different substrate specificity observed for AKR7A5, a member of the SSA reductases (group II), and AKR7A1, the original aflatoxin reductase (group I).

MATERIALS AND METHODS

Expression and Purification of Recombinant AKR7A Enzymes. Mouse AKR7A5 was expressed from IPTG-inducible expression plasmids in *Escherichia coli* BL21 pLysS as described previously (*9*, *15*). The BL21 pLysS cells were harvested by centrifugation, frozen at −80 °C, and then lysed with a French press in lysis buffer [20 mM sodium phosphate (pH 7.4) and 0.5 M NaCl]. The extract was loaded on a 5 mL Ni$^+$ HiTrap chelating affinity column (Amersham Life Sciences) to purify the His$_6$-tagged AKR7A5. The purity of the eluted AKR7A5 was verified by SDS−PAGE and its concentration by the Bradford assay (*20*).

Crystallization. Purified AKR7A5 was desalted and concentrated to 15 mg/mL using Centricon-10 centrifugal concentrators (Amicon) into 20 mM Tris-HCl (pH 7.5) and 0.5 mM dithiothreitol. The protein was supplemented with 1 mM NADP$^+$, and crystallization trials were set up using the sitting-drop vapor-diffusion method at 20 °C. A number of crystallization conditions were identified from commercial and in-house sparse matrix screens. Linear optimization of crystallization conditions and subsequent preliminary X-ray analysis identified diffraction quality crystals. The best crystals were obtained by equilibrating a mixture of 2 μL of protein solution [15 mg/mL AKR7A5, 20 mM Tris-HCl (pH 7.5), 0.5 M dithiothreitol, and 1 mM NADP$^+$] and 2 μL of precipitant solution [0.2 M sodium tartrate, 7.5% PEG8000, and 0.1 M MES-NaOH (pH 6.5)]. Needlelike crystals formed within a few hours and grew to a maximum size of 0.07 mm × 0.07 mm × 0.5 mm after 1 week.

Data Collection. The diffraction data of AKR7A5 were collected at Daresbury SRS station 9.6 using a CCD (ADSC) Quantum 4 detector. A solution of 8% PEG8000, 0.1 M MES (pH 6.1), 0.2 M sodium tartrate, and 20% glycerol was added to the crystallization drop. Crystals were mounted in Hampton Research cryoloops and flash-frozen at 100 K. Data were collected from a single crystal in a single pass using the 1° oscillations. Data for AKR7A5 were integrated and scaled using the HKL suite of programs (*21*). The data were initially indexed in a *C*-centered monoclinic space group, but it became apparent during scaling based on the merging *R*-factor and the number of rejections that the true space group was *P*1. The data were reprocessed with the following unit cell dimensions: $a = 98.47$ Å, $b = 159.17$ Å, $c = 96.64$ Å, $\alpha = 90.0°$, $\beta = 119.38°$, and $\gamma = 78.53°$ in *P*1 with an *R*-merge of 10.8% to 2.3 Å; however, the data were weak with an average $I/\sigma I$ of slightly greater than 1 in the 2.38−2.3 Å shell. On the basis of *R*-merge statistics and $I/\sigma I$, the data should be considered good to ~2.5 Å resolution; however, the weak data were included to 2.3 Å in the refinement. The CCP4 suite of programs (*22*) was used to convert integrated intensities to structure factor amplitudes, and 5% of the reflections were set aside for use in R_{free} calculations. The data processing statistics are summarized in Table 1.

Table 1: Data Collection and Refinement Statistics

	AKR7A5
crystal data	
space group	*P*1
unit cell dimensions	$a = 98.469$ Å, $b = 159.170$ Å, $c = 96.636$ Å, $\alpha = 90.00°$, $\beta = 119.38°$, $\gamma = 78.53°$
no. of molecules in the asymmetric unit	10
data processing	
resolution (Å)	42−2.5
total no. of reflections	497885
no. of unique reflections	170033
multiplicity^{a,b}	2.9 (2.9)
overall I/σ^{b}	4.1 (2.4)
completeness (%)^{b}	98.8 (98.4)
R_{merge} (%)^{b,c}	8.7 (47.7)
Wilson *B* (Å^2)	41.0
refinement	
resolution (Å)	30−2.3
R_{work} (%)^{d}	17.0 (27.0)
R_{free} (%)^{d}	22.2 (34.6)
coordinate error (Å)	0.2
rms deviation	
bond lengths (Å)	0.032
bond angles (deg)	2.4
mean *B* factor (Å^2)	33.9
Ramachandran quality (%)	
most favored region	90.9
Allowed regions	9.1
Disallowed	0.3

[a] Redundancy of data, defined as the ratio of the number of measured and the number of unique reflections. [b] Values for data in parentheses for the final resolution shell (2.54−2.50 Å). [c] $R_{\text{merge}} = \sum_h \sum_i |I(h,i) - \langle I(h)\rangle| / \sum_h I(h,i)$, where $I(h,i)$ is the intensity value of the *i*th measurement of *h* and $\langle I(h)\rangle$ is the corresponding mean value of *h* for all *i* measurements of *h*; R_{merge} is therefore the summation over all measurements. [c] $R = \sum_{hkl}(|F_o - F_c|)/\sum|F_o|$. Weak data were included to 2.3 Å, and statistics are quoted in parentheses for the resolution range of 2.38−2.30 Å.

Structure Solution and Refinement. AKR7A5 was determined by molecular replacement with the stand-alone version of AMoRe (*23*) using a symmetrical dimer generated from rat liver AKR7A1 (chain A of PDB entry 1GVE, the NADP$^+$-bound form of the enzyme) as the search model (*9*) and X-ray data between 10 and 4 Å resolution. We searched for six dimers on the basis of a Matthews number (*24*) of 2.85 giving a solvent content of roughly 50%. However, an unambiguous solution was found for five dimers (Matthews number of 3.42, 64% solvent content), which after rigid body refinement gave a correlation coefficient of 57.5% and an *R*-factor of 35.9%. Refinement was carried out using REFMAC5 (*25*) with all data between 30 and 2.3 Å using tight noncrystallographic symmetry (NCS) restraints reducing R_{work} to 25.2% and R_{free} to 29.9%. The 10-fold NCS-averaged electron density maps were calculated, and correction of the model was carried out on a single monomer using QUANTA (Accelrys, San Diego, CA). The corrected model was used to generate the other nine monomers in the asymmetric unit by application of the NCS matrices. A model of a tartrate molecule was produced and fitted into the electron density in the active site of the structure using X-LIGAND (Accelrys). Waters were added into the $|F_o| - |F_c|$ density map at $>3\sigma$ and within 2.95 Å of the hydrogen bonding partner using X-SOLVATE. In the latter stages of refinement, six phosphate ions and 25 glycerols were identified and included. After the inclusion of TLS refinement for each individual monomer, the refinement was considered complete when further rebuilding and REFMAC5 cycles failed to decrease R_{free}.

Site-Directed Mutagenesis. The QuickChange site-directed mutagenesis kit (Stratagene) was used to introduce V44M, M77W, and F224W mutations into AKR7A1 expression plasmid pEE65 (*11*), using the following primers: V44M, 5′-dAGATAGACACCGCCTTCATGTATGCGAACGGTC-3′ and 5′-dCTGACCGTTCGCATACATGAAGGCGGTGTCTAT-3′; M77W, 5′-dCCACCAAGGCTGCCCCATGGTTTGGGAAGACACTG-3′ and 5′-dCAGTGTCTTCCCAAACCATGGGGCAGCCTTGGTGG-3′; and F224W, 5′-dGCTTCTTTGGGAATCCATGGTCTCAACTGTACATGGAC-3′ and 5′-dGTCCATGTACAGTTGAGACCATGGATTCCCAAAGAAGC-3′.

The underlined bases represent the mutated codons. The complete coding regions of the mutated plasmids were sequenced to ascertain the fidelity of the mutant construct.

Enzyme Assays. Enzymatic activities toward SSA were measured with a Beckman DU650UV or Shimadzu UV-2401PC single-beam recording spectrophotometer by monitoring the decrease in absorbance at 340 nm caused by the oxidation of cofactor NADPH ($\epsilon = 6270\ \mathrm{M^{-1}\ cm^{-1}}$). The initial velocity of the reaction was assayed at 25 °C in a 1 mL mixture containing 100 mM sodium phosphate buffer (pH 6.6), a series of concentrations of SSA, and 100 μM NADPH. The assays were initiated by the addition of the purified enzyme to the reaction mixture. The nonenzymatic rate was subtracted from the measurement, and nonlinear regression software, Graphpad Prism 4, was used to calculate the kinetic parameters k_{cat} and K_m toward SSA.

RESULTS AND DISCUSSION

Crystal Structure of AKR7A5

Overall Structure. The data reduction and refinement statistics for the model are summarized in Table 1. The structure contains 10 protein subunits in the asymmetric unit, all of them occupied by cofactor NADP$^+$ and an inhibitor tartrate (derived from the crystallization conditions) forming the ternary complex. The N-terminus of AKR7A5 is disordered in the structure and not visible in the electron density; this includes the polyhistidine tag and the first 14 amino acid residues of the native protein (MSRPPPPRAASGAP). The amino acid sequence of AKR7A5 is numbered according to the sequence of AKR7A1 described previously (*9*).

AKR7A5 has a typical AKR7 family fold, common to all the members of the aldo-keto reductase superfamily, comprising a $(\beta/\alpha)_8$ barrel with two additional α-helices, H1 and H2, which are associated with the C-terminal portion of the protein (Figure 1). The key loops which are important for substrate specificity in the family 1 enzymes of the aldo-keto reductase superfamily (which are the most heavily studied) are named loops A−C (Figure 1). Like AKR7A1 (*9*) and AKR2B5 (*26*), AKR7A5 is dimeric. The dimer is symmetrical, both monomers having tartrate and NADP$^+$ bound, unlike the previously described AKR7A1 structure where one subunit is the ternary complex and the other the apoenzyme (*9*). There is only one significant difference in the composition of the dimer interface between AKR7A1 and AKR7A5, namely, that Lys155, which forms a salt bridge with Glu118 in AKR7A1, is a serine in AKR7A5; therefore, both the buried surface area and a charged interaction are lost.

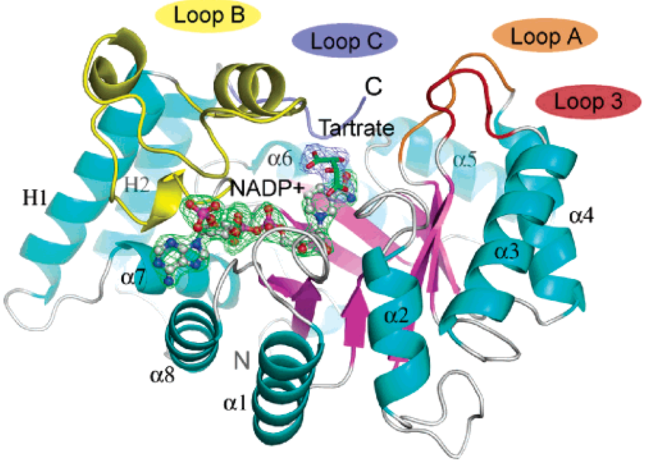

FIGURE 1: Ribbon diagram of the ternary complex of mouse AKR7A5, with α-helices colored cyan (and labeled) and β-strands colored magenta. The classic AKR loops are highlighted [loop A (orange), loop B (yellow), and loop C (blue)], along with loop 3 (red), which has been shown to be important in AKR7 family enzymes. Cofactor NADP$^+$ is shown as a ball-and-stick model, and tartrate is shown in stick format colored by atom type. Unaveraged omit map electron density (corresponding to chain A) is shown for NADP$^+$ (green) and tartrate (blue) contoured at 3.5σ. This figure was produced using PYMOL from DeLano Scientific (San Carlos, CA).

NADP$^+$ Binding. The NADP$^+$ cofactor binds in an extended conformation in a deep cleft of AKR7A5 in a fashion similar to that observed in AKR7A1 (*9*) (Figure 1). The cofactor makes numerous contacts with the protein, with the nicotinamide ring being bound in the core of the β/α barrel, the pyrophosphate group between β-strands $\beta7$ and $\beta8$, and the AMP moiety among α-helices α7 and α8 and loop B. Differences between the AKR7A1 structure and the AKR7A5 structure reported here are in the adenine moiety of the cofactor. In terms of changes in amino acid sequence, there is a lysine at position 204 in AKR7A5 instead of an arginine. This lysine forms a single charged interaction with a hydrogen bond to the 2′-monophosphate and a hydrogen bond to the adenine ring. The 2′-monophosphate moiety is moved relative to the AKR7A1 structure with the phosphate oxygen atoms rotated ∼30° around the phosphorus atom. This results in better hydrogen bonding among Gln290, Ser286, and the 2′-monophosphate (2.8 and 2.6 Å distances, respectively) and worse interactions between Arg18, which is not well-ordered, and Arg218 (both 3.2 Å in distance). These changes are minor, however, and it is unlikely that these would make a significant difference in the affinity of AKR7A5 for the cofactor. The residues that bind the nicotinamide moiety of the cofactor are highly conserved between AKR family members (*9*, *10*). The nicotinamide ring forms a $\pi-\pi$ stacking interaction with the side chain of Tyr193 and orients the stereochemistry of hydride transfer

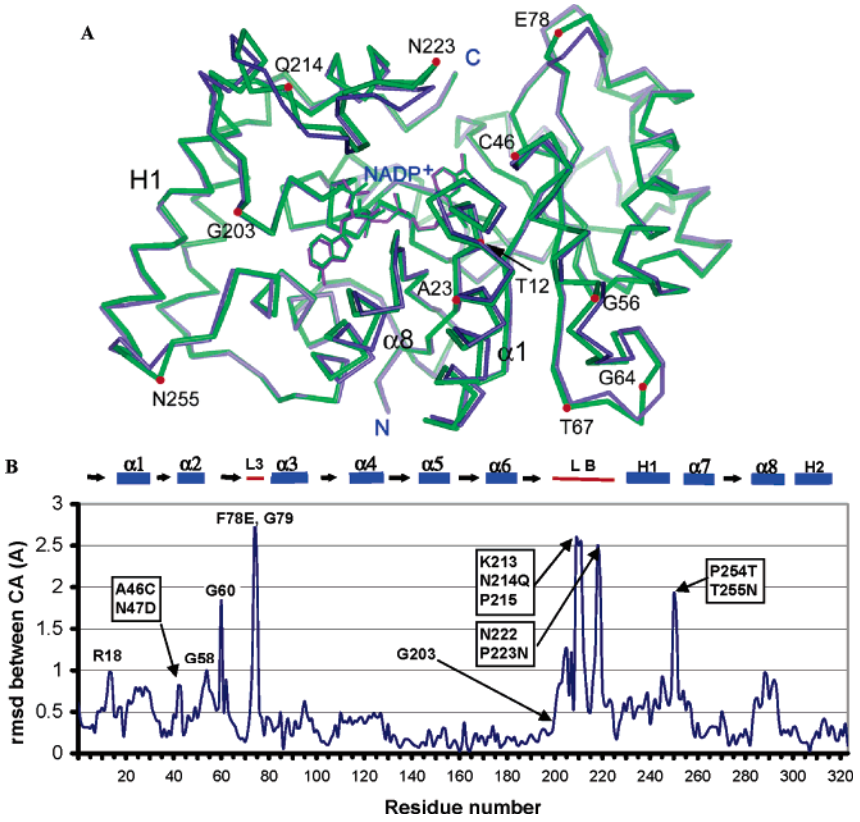

FIGURE 2: (A) Superposition of the rat liver AKR7A1 structure (purple) and mouse AKR7A5 structure (green) represented as a CA trace. The largest differences between the structures are highlighted with a red dot and labeled using the AKR7A5 numbering. Secondary structure elements that have moved are also labeled. (B) Plot of the root-mean-square deviation (rmsd) in CA position between AKR7A1 and AKR7A5 vs residue number. The secondary structure is shown for clarity with α-helices represented as rectangles, β-strands as arrows, and significant loops as lines; both helices and loops are labeled. On the rmsd plot, the largest differences in CA position are labeled, and if sequence differences exist, these are shown with the AKR7A5 amino acid residue labeled first and AKR7A1 last.

with the assistance of a network of three hydrogen bonds between the C3 carboxamide group and the side chains of Ser139, Asn140, and Gln165. These interactions control the 4-*pro-R* hydride transfer from the A face of the nicotinamide ring of NADPH to the substrate. A feature of the group I enzymes (AKR7A1) is the presence of a phenylalanine at position 193 instead of a tyrosine, and as a result, hydrogen bonds between the terminal hydroxyl and the side chains of Asn140 and Arg327 are lost (2.5 and 3.0 Å in length, respectively), and the phenyl ring is moved 0.3 Å away from these groups. It is possible that this change has more to do with the orientation of Arg327, a residue implicated in substrate binding, than with any specific effect on the cofactor.

Active Site. The residues implicated in catalysis for the AKR superfamily are conserved in the active site of AKR7A5. The individual roles of the four residues (Asp40, Lys73, Tyr45, and His109) are as follows: Tyr45 and His109 bind the aldehyde or ketone group of the substrates, Tyr45 acts as the proton donor during the reduction reaction, while the Asp40−Lys73 salt bridge modulates the pK_a of the tyrosine. Besides the catalytic tetrad, residues from loops A−C define the active center of AKR enzymes in general. However, in AKR7 family enzymes, loop A is significantly smaller than other mammalian AKR enzymes which belong to the AKR1 family, e.g., aldose reductase. Instead, the amino acid residues that are normally contributed by loop A are in fact contributed in AKR7 enzymes by an equivalent loop from the preceding β-strand, which is called loop 3 (Figure 1).

There are a number of relatively small changes in the main conformation between the AKR7A5 and AKR7A1 ternary complex structures (Figure 2). Between residues 80 and 200 of the two protein structures, the difference in CA position is on the order of the coordinate error and therefore is considered to be identical (Figure 2B). If one starts from the N-terminus, the first significant difference between the two structures is the loop between strand β1 and helix α1 which is largest at Arg18. Despite the sequences being identical, there are large changes in the positions of Arg17 and Arg18. These differences in conformation are probably the result of the change from Ala12 (AKR7A1) to Thr (AKR7A5) before the loop and a series of sequence changes after the loop, e.g., Val21 to Ala. In addition, the adjacent loop has the sequence change from Ala46 to Cys, and this would form a short contact to CB of Arg17 (∼2.7 Å) and therefore is instrumental in the conformational differences both in the first loop and in the residues around residue 46. Helices α1 and α8 shift concertedly relative to the rest of the structure, arguably as the result of sequence differences in the residues that form the hydrophobic core of the enzyme in this region. Significant sequence differences in residues 56 and 67 which form the large turn between helix α2 and strand β2 result in changes in the two structures, the largest of which is the result of the change of Ser64 to Gly (Figure 2A). A smaller loop (residues 254 and 255) between α-helices H1 and α7 also has a changed conformation due to sequence differences between AKR7A1 and AKR7A5 (Figure 2). These differences are to be expected and are far

```
A
                  * a bc           Group
Mouse AKR7A5  KIATKANPWEGKSLK 123  II
Human AKR7A2  KIATKANPWDGKSLK 94   II
Rat   AKR7A4  KIATKANPWDGKSLK 123  II
Dog1          KIATKANPWEGKSLK 114  II
Bovine1       KIATKANPWEGKSLK 110  II
Frog1         KMATKANPWGGNTLK 110  II
Chicken1      EVATKANPWEGNTLK 19   II
Pufferfish1   SVATKANPWDGKTLK 79   II
Zebrafish1    RIATKANPWEGKTLK 79   II

Rat   AKR7A1  KIATKAAPMFGKTLK 83   I
Human AKR7A3  KIDTKAIPLFGNSLK 87   I
Chimp1        KIDTKAIPLFGNSLK 26   I

B
                           d    e          Group
Mouse AKR7A5  QPVGRFFGNNWAETYRNRFWKEHHF 278  II
Human AKR7A2  QPEGRFFGNSWSETYRNRFWKEHHF 249  II
Rat   AKR7A4  QPEGRFFGNSWSETYRNRFWKEHHF 278  II
Dog1          QPVGRFFGNNWAETYRNRFWKEHHF 269  II
Bovine1       QPLGRFFGNSWAEVYRNRYWKEHHF 265  II
Frog1         QASCRFFGNSWAEVYRNRYWKKHHF 265  II
Chicken1      QPTGRFFGNDWAQAYRDRYWKKHNF 174  II
Pufferfish1   QPAGRFFGNSWAKAYQDRYWKKSHF 234  II
Zebrafish1    QPAGRFFGNNWANAYRDRYWKESHF 234  II

Rat   AKR7A1  NPESRFFGNPFSQLYMDRYWKEEHF 238  I
Human AKR7A3  QPVGRFFGNTWAEMYRNRYWKEHHF 242  I
Chimp1        QPVGRFFGNTWAEMYRNRYWKEHHF 205  I
```

FIGURE 3: AKR7-related proteins from higher eukaryotes. Characterized enzymes are shown in bold. Putative proteins predicted from genome sequencing projects are shown in normal font. (A) Differences in loop 3 between group I and group II AKR7 enzymes are (a) Asn vs Ala/Ile, (b) Trp vs Met/Leu, and (c) Glu/Asp vs Phe. The lysine involved in the catalytic tetrad is denoted with an asterisk. (B) Differences in loop B between group I and group II AKR7 enzymes are (d) Leu/Met vs Thr/Ala/Val and (e) Tyr vs Phe; however, this is not conserved when all AKR7-related proteins are considered.

from the active site and not expected to play a role in the kinetic properties of the two enzymes. By far the largest differences seen between the two enzymes are in loop 3 and loop B, both of which are close to the active site and play a role in substrate specificity.

In AKR7A5, there are four differences in the sequence within loop 3, three of which are changes seen to occur between members of group I and group II AKR7A enzymes, namely, Asn75Ala, Trp77Met, and Glu78Phe (Figure 3A). Additionally, there are three changes in sequence between AKR7A1 and AKR7A5 at the beginning of helix α3 which follows the loop, but these are differences seen mainly between AKR7A1 and other AKR7A family members. The substitution of Phe78 for a Glu/Asp removes favorable van der Waals interactions of this side chain with Val44 and probably results in the movement of the main chain of loop 3 at this residue (Figure 4A). Other changes in the main chain conformation of loop 3 are the result of the Asp86Ser change at the beginning of helix α3. The presence of an Asp in AKR7A1 results in a peptide flip in residue Lys80 to avoid a steric clash and permit Asp86 to hydrogen bond to the amide nitrogen of Thr81. The side chain of Lys80 is able to adopt a different conformation and forms hydrogen bonds to the R group of Asn75 and the amide oxygen of Trp77 (Figure 4A). This undoubtedly further effects the conformation of the loop which results in Trp77 of AKR7A5 being positioned farther into the active site cavity than Met77 in AKR7A1. Thus, Trp77 in AKR7A5 occupies a position halfway between Met77 in AKR7A1 and Phe110 (the residue that immediately follows the catalytic histidine) on the adjacent β-strand, which in AKR7A5 and other group II AKR7A enzymes is always an alanine.

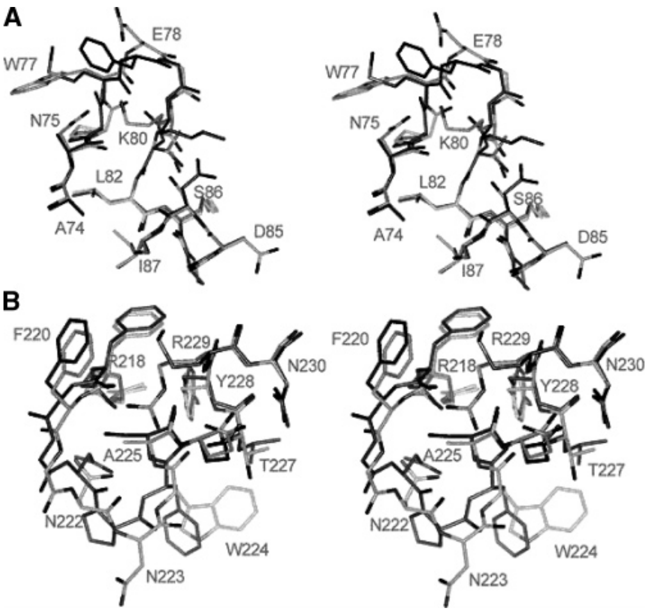

FIGURE 4: Stereodiagrams comparing the structures of (A) loop 3 and (B) loop B in AKR7A1 (carbons colored dark gray) and AKR7A5 (carbons colored light gray).

With respect to loop B, both R218 and Tyr228 which are involved in binding the cofactor and substrate or inhibitor, respectively, occupy almost identical orientations in the two AKR7 enzyme structures. In total, between AKR7A1 and AKR7A5 there are 11 amino acid differences between the two proteins in loop B, only two which are consistently different between group I and group II AKR7A enzymes, namely, Leu227Thr and Tyr232Phe (Figure 3B). Given the proximity of a number of residues in loop B to the active site, it is probable that, for example, Trp224, which is Phe in AKR7A1, will have an effect on substrate specificity (Figure 4B). Of the consistent changes, Tyr232 in AKR7A1 is Phe232 in AKR7A5 and as a result loses two hydrogen bonds with Asn169 and Asn194. It is expected that this may have an effect on the dynamics of lid closure and potentially the precise orientation of active site residues by loosening the structure somewhat. When the amino acid sequences of all AKR7-like proteins are considered, it becomes clear that the Tyr232Phe difference between group I and group II enzymes is not conserved. Therefore, it is unlikely that this change should have a direct effect on substrate specificity and particularly SSA binding.

Considering the differences between AKR7A5 and AKR7A1, it seems that the changes that have a large effect on the active site cavity are Trp224 in loop B which lies flat over the active site of AKR7A5 and the introduction of the bulky hydrophobic residues Trp77 (loop 3) and Met44 (directly before the catalytic tyrosine) into the active site cavity. Together, these three residues produce a smaller active site cavity more favorable to the binding of a substrate such as SSA.

Probing the Active Site Using Site-Directed Mutagenesis

Several differences between AKR7A1 and AKR7A5 enzyme structures occur within the active site and in the proximity of the substrate analogue inhibitors. These include M77W, V44M, and F224W. These combine to reduce the size of the substrate binding pocket of AKR7A5 compared

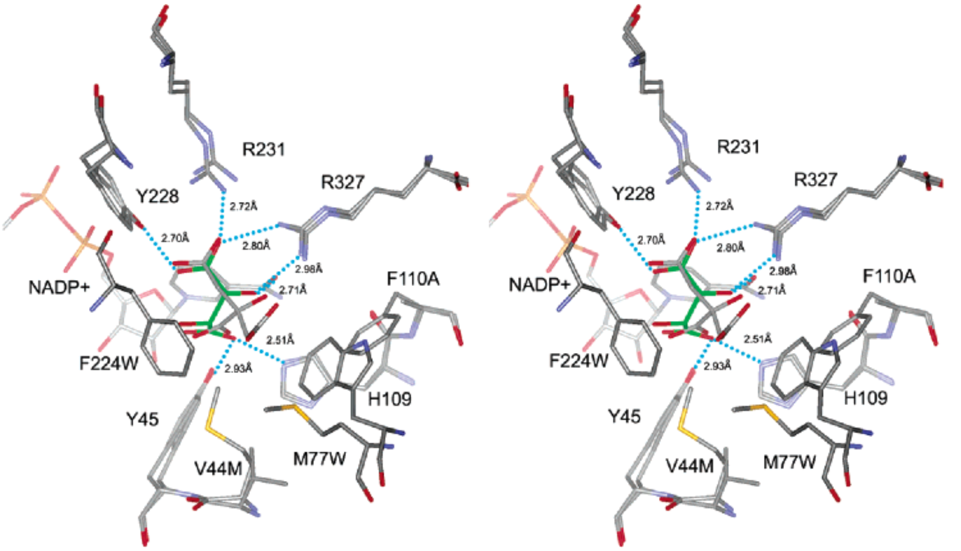

FIGURE 5: Superposition of the residues involved in substrate binding of AKR7A1 and AKR7A5. The protein amino acid residues are colored according to atom type and labeled with AKR7A1 first and AKR7A5 last when there are differences. Only Trp224 is omitted for clarity as the indole ring lies directly over the tartrate molecule. Hydrogen bonds from AKR7A5 to tartrate (carbons colored green) are shown as dotted blue lines with hydrogen bond distances given.

Table 2: Kinetic Parameters of Wild-Type AKR7A Enzymes and AKR7A1 Mutants for SSA

sample	k_{cat} (min^{-1})	K_m (μM)	k_{cat}/K_m (min^{-1} μM^{-1})
AKR7A5	121.6 ± 1.0	19.8 ± 0.5	6.14
AKR7A1	108.0 ± 3.6	217.0 ± 18.6	0.50
V44M	80.4 ± 4.3	97.2 ± 12.5	0.83
M77W	68.7 ± 2.8	46.5 ± 5.8	1.48
F224W	66.3 ± 3.4	148.0 ± 16.1	0.47

to that of AKR7A1 (Figure 5), accounting for the higher affinity of AKR7A5 for SSA versus AKR7A1.

Single-site mutations of a number of active site residues were carried out to test their effect on SSA binding. Three mutants of AKR7A1 were constructed (V44M, M77W, and F224W) and enzymes expressed and purified as previously described for the wild-type enzymes (*9*, *15*). All mutant enzymes were expressed at high levels, and no significant protein degradation occurred during their purification and storage, which indicated that the introduced mutations do not affect stability.

Kinetic Parameters of the Wild Type and the Mutants for Succinic Semialdehyde (SSA)

The kinetic data of wild-type enzymes and mutants for SSA are summarized in Table 2. Wild-type AKR7A1 has a k_{cat} for SSA similar to that of AKR7A5, but the specificity constant k_{cat}/K_m of AKR7A1 is less than one-tenth of that of AKR7A5, due to the much lower affinity for SSA, shown by the higher K_m value. For the wild-type AKR7A enzymes and all the mutants that were tested, the k_{cat}/K_m values are at most 10^5 M^{-1} s^{-1}. As the k_{cat}/K_m is much lower than 10^9 M^{-1} s^{-1}, it is reasonable to conclude that an equilibrium mechanism is more appropriate than a steady-state mechanism (*27*). This means that the observed K_m approximates the dissociation constant of the enzyme−substrate complex and, therefore, reflects the affinity of the enzymes for these substrates.

Considering the K_m values, the mutants V44M, M77W, and F224W improve the affinities for SSA between 2- and 5-fold, while k_{cat} remains roughly the same. Overall, mutants V44M and M77W improve the specificity constant toward SSA by 1.7- and 3-fold, respectively, which indicates the importance of these two residues for the proposed function of the enzyme as a SSA reductase. These two residues, therefore, appear to be important specificity determinants of AKR7A5. The Val44Met mutation introduces a bulky hydrophobic residue into the active site, reducing the size of the substrate binding pocket and increasing the number of favorable van der Waals contacts with substrate. However, in the AKR7A1 Met77Trp mutant if the tryptophan were to adopt the same conformation as seen in the AKR7A5 structure (Figure 5), a serious steric clash would occur with Phe110 (which is invariantly an alanine in type II AKR7 enzymes). An alternative conformation of either Phe110 or Trp77 must occur; either way, the Trp residue should extend into the substrate binding pocket and restrict the size of the substrate binding pocket, accounting for the improved stability of SSA binding.

Inhibitor Binding and Substrate Specificity. The structure of AKR7A1 in complex with citrate and NADP$^+$ (*9*) together with the tartrate-bound ternary complex of AKR7A5 reported here allows comparison of the mode of inhibitor binding and the arrangement of amino acid residues in the binding pocket of the two enzymes. Although the structures of citrate and tartrate differ slightly in size and chemical functionality, these two inhibitors bind to equivalent residues in AKR7A1 and AKR7A5 (Figure 5). As seen in other AKR−inhibitor complexes, carboxylate groups bind to the active site in the anion hole created by the side chains of the catalytic histidine (His109), tyrosine (Tyr45), and N4 of the nicotinamide ring of NADP (*28*−*30*). In both structures, one oxygen atom of citrate and tartrate are superposed within 0.3 Å and occupy the presumed position of the aldehyde or ketone group of the physiological substrates. In addition, in AKR7A1 the hydroxyl group of citrate hydrogen bonds with the oxygen NO7 of the NADP$^+$ amide and to the side chain NH$_2$ group of Arg327, in the same way as the C3 hydroxyl of tartrate binds in the AKR7A5 structure (Figure 5). Of the two acetate

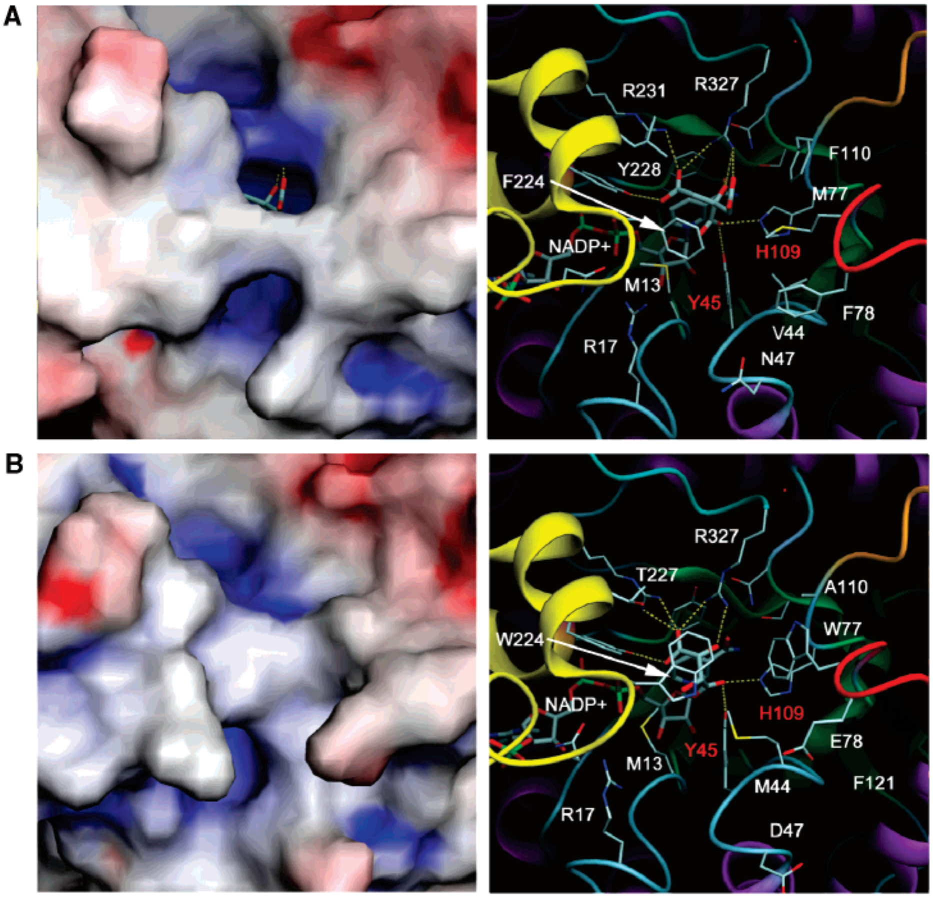

FIGURE 6: Detailed views of the substrate binding pocket of AKR7A5 (A) and AKR7A1 (B). The left-hand frame is a surface representation of the enzyme colored according to electrostatic potential with blue representing positive potential and red negative potential. The right-hand frame is a detail of the same view with β-strands colored green, α-helices purple, loop A orange, loop B yellow, loop C cyan, and a short loop between strand β3 and α3 red. Residues are colored according to atom type. The inhibitors tartrate and citrate together with the NADP$^+$ cofactor are both shown as thicker sticks than the protein side chains. The catalytic tyrosine and histidine are labeled in red for clarity. The diagram was produced using DINO.

moieties in citrate, one is buried in the active site of AK7A1 and forms hydrogen bonds with the side chains of Arg231, Tyr228, and Arg327 together with an electrostatic interaction. The second carboxyl in tartrate forms essentially the same interaction with side chains in AKR7A5 as the acetate moiety of the citrate in AKR7A1. These conserved interactions between the inhibitors and the active sites of AKR7A1 and AKR7A5 are likely to represent residues that play key roles in binding substrates.

Citrate and tartrate seem to form essentially the same interactions in AKR7A1 and AKR7A5; however, the main body of the two inhibitors adopts different orientations in the active site. The most likely reason for this is the C3 hydroxyl of tartrate, which although adopting a position similar to that of the hydroxyl group of citrate is not in an equivalent position within the molecule (Figure 5). As a result, the C1 carboxylate group of tartrate is rotated approximately 30° around the oxygen that is within the carboxy anion hole. This has two effects. First, C2 is moved 1.4 Å away from the equivalent carbon in citrate; second, the second oxygen of the C1 carboxylate is moved into an unfavorable position where it makes close contacts with CE of Met13 (2.7 Å) and CE1 of the phenyl ring of Tyr45 (3.1 Å). These close contacts are associated with shifts in the two amino acid side chains to minimize the steric clash; for example, Met13 adopts a different rotamer conformation (Figure 6). Although tartrate has a hydroxyl at C2, it is in the up position and therefore unable to make the favorable hydrogen bond interactions with the amide of the nicotinamide ring and the side chain of Arg327. The hydroxyl at C3 is, however, in the down position and therefore able to form these hydrogen bonds which are comparable in angle and length to those seen in the the AKR7A1−citrate structure. Although the C4 carboxylate of tartarte forms hydrogen bonds equivalent to those seen in the AKR7A1−citrate structure, the equivalent carboxylate carbon atom in citrate is 0.4 Å above and therefore alters slightly the angle of the hydrogen bonds that are formed.

Table 3: Inhibition of AKR7 Enzymes by Different Ligands

	K_{ESI} (μM)			
enzyme	succinate	citrate	tartrate	*N*-formylglycine
AKR7A1	320 ± 20	160 ± 8	840 ± 50	7400 ± 1700[a]
AKR7A5	120 ± 7	100 ± 6	810 ± 60	850 ± 50

[a] Mixed inhibition.

Kinetic characterization of citrate, tartrate, and succinate as inhibitors of AKR7A5 and AKR7A1 with SSA as a substrate showed that the inhibition is uncompetitive and that citrate is a good inhibitor of both enzymes having K_{ESI} values of 160 and 100 μM, respectively (Table 3). As AKR7A5 is a much better SSA reductase than AKR7A1, succinate was expected to be a better inhibitor for this enzyme with a K_{ESI} of 120 μM compared to a K_{ESI} of 320 μM for AKR7A1. However, that tartrate should be a much poorer inhibitor of both enzymes was a surprise ($K_{ESI} \sim 820$ μM for both enzymes). In light of the data from the crystal structure of AKR7A5 in complex with tartrate, it seems clear that the unfavorable interactions formed by the carboxylate at C1 in tartrate offset favorable interactions formed by the C3 hydroxyl and C4 carboxyl and therefore reduce the affinity of the inhibitor for the enzyme.

A comparison of the K_{ESI} of succinate (120 μM) with the K_m of AKR7A5 for SSA (19 μM) suggests it is probable that there are still some steric effects introduced by the oxygen of the C1 carboxylate of succinate compared to the hydrogen in SSA. In an attempt to investigate this possibility, *N*-formylglycine was investigated as a potential inhibitor, with the expectation that it could mimic the aldehyde substrate without itself being a substrate. However, the inhibition of AKR7A5 by *N*-formylglycine was equivalent to that of tartrate ($K_{ESI} \sim 820$ μM) and almost 10-fold worse for the AKR7A1 enzyme ($K_I \sim 7400$ μM). The most logical explanation is that the introduction of planarity over the amide group does not permit the optimal binding of the carboxylate group and amide oxygen in the active site.

CONCLUSIONS

We have reported the crystal structure of AKR7A5 in complex with NADP$^+$ and tartrate and have shown small conformational differences between this structure and that of AKR7A1 within the active site. Only one side of the active site has a significant number of amino acid changes; these are directly above the catalytic residues Tyr45 and His109 and most notably involve changes in loop 3 (Figure 6). These changes undoubtedly restrict the active site cavity, adding favorable van der Waals interactions between the substrate and protein. However, the key hydrogen bond and charged interactions are retained between the two AKR7 enzymes, suggesting similar substrates will be metabolized. This is consistent with the idea that one of the AKR7A genes in rat and humans arose through a gene duplication event. The acquisition of a second AKR7A enzyme in these species allowed the development of a more specialized enzyme. Given that the AKR7A1 enzyme is inducible, it is likely that this enzyme arose after the SSA reductase, with a more specialized role in detoxification. The fact that mouse possesses only one enzyme suggests that the specialized version of AKR7A was not required, possibly because other detoxification enzymes were able to carry out the functions that AKR7A1 performs in rat.

Comparison of the crystal structures of AKR7A5 and AKR7A1 has identified three amino acid residues which could act as determinants of SSA specificity. Mutation of these residues in AKR7A1 to those found in AKR7A5 was expected to improve the specificity of AKR7A1 for SSA. Two of the three mutants improved the specificity with the Met77Trp mutant showing a 3-fold improvement. However, the improvement in the binding of SSA by each of the three mutants was offset by a reduction in the catalytic efficiency of 26% (Val44Met) to 38% (Phe224Trp). It is clear that the next step to improve the specificity of AKR7A1 for SSA further it will be necessary to combine multiple point mutations to arrive at a minimal subset of SSA specific determinants.

The AKR7A5 structure reported here is in complex with the inhibitor tartrate, which proves to be a poor inhibitor of both AKR7 enzymes that were studied. So far, only succinate citrate and indomethacin have been shown to be effective inhibitors, and these show no selectivity and are only modest inhibitors of both enzymes (*16*, *17*). *N*-Formylglycine which is characterized here, while exhibiting almost 10-fold selectivity for AKR7A5 over AKR7A1, is a much poorer inhibitor than either citrate or succinate. The availability of crystal structures of a group II enzyme from mouse will pave the way for the development of selective AKR7 inhibitors. These are required to better understand the roles of the group I and group II enzymes in vivo and may have potential therapeutic benefits in the prevention of GHB accumulation from SSA.

REFERENCES

1. Rondeau, J., Tete-Favier, F., Podjarny, A., Reymann, J., Barth, P., Biellman, J., and Moras, D. (1992) Novel NADPH-binding domain revealed by the crystal structure of aldose reductase, *Nature 355*, 469−472.
2. Wilson, D. K., Bohren, K. M., Gabbay, K. H., and Quiocho, F. A. (1992) An unlikely sugar substrate site in the 1.65 Å structure of the human aldose reductase holoenzyme implicated in diabetic complications, *Science 257*, 81−84.
3. Hoog, S., Pawlowski, J., Alzari, P., Penning, T., and Lewis, M. (1994) Three-dimensional structure of rat liver 3a-hydroxysteroid/dihydrodiol dehydrogenase: A member of the aldo-keto reductase superfamily, *Proc. Nat. Acad. Sci. U.S.A. 91*, 2517−2521.
4. El Kabbani, O., Judge, K., Ginell, S. L., Myles, D. A., DeLucas, L. J., and Flynn, T. G. (1995) Structure of porcine aldehyde reductase holoenzyme, *Nat. Struct. Biol. 2*, 687−692.
5. Wilson, D. K., Nakano, T., Petrash, J. M., and Quiocho, F. A. (1995) 1.7-Angstrom Structure of Fr-1, a Fibroblast Growth Factor-Induced Member of the Aldo-Keto Reductase Family, Complexed with Coenzyme and Inhibitor, *Biochemistry 34*, 14323−14330.
6. Khurana, S., Powers, D. B., Anderson, S., and Blaber, M. (1998) Crystal structure of 2,3-diketo-D-gluconic acid reductase A complexed with NADPH at 2.1-Å resolution, *Proc. Natl. Acad. Sci. U.S.A. 95*, 6768−6773.
7. Ye, Q., Hyndman, D., Li, X., Flynn, G. T., and Jia, Z. (2000) Crystal structure of CHO reductase, a member of the aldo-keto reductase superfamily, *Proteins 38*, 41−48.
8. Hur, E., and Wilson, D. K. (2000) Crystallization and aldo-keto reductase activity of Gcy1p from *Saccharomyces cerevisiae*, *Acta Crystallogr. D56*, 763−765.
9. Kozma, E., Brown, E., Ellis, E. M., and Lapthorn, A. (2002) The Crystal Structure of Rat Liver AKR7A1. A dimeric member of the aldo-keto reductase superfamily, *J. Biol. Chem. 277*, 16285−16293.
10. Kozma, E., Brown, E., Ellis, E. M., and Lapthorn, A. J. (2003) The high-resolution crystal structure of rat liver AKR7A1: Understanding the substrate specificites of the AKR7 family, *Chem.-Biol. Interact. 143−144*, 289−297.
11. Ellis, E. M., Judah, D. J., Neal, G. E., and Hayes, J. D. (1993) An ethoxyquin-inducible aldehyde reductase from rat liver that metabolizes aflatoxin B_1 defines a subfamily of aldo-keto reductases, *Proc. Natl. Acad. Sci. U.S.A. 90*, 10350−10354.
12. Ireland, L. S., Harrison, D. J., Neal, G. E., and Hayes, J. D. (1998) Molecular cloning, expression and catalytic activity of a human AKR7 member of the aldo-keto reductase superfamily: Evidence that the major 2-carboxybenzaldehyde reductase from human liver is a homologue of rat aflatoxin B_1 aldehyde reductase, *Biochem. J. 332*, 21−34.
13. Knight, L. P., Primiano, E. A., Groopman, J. D., Kensler, T. W., and Sutter, T. (1999) cDNA cloning, expression and activity of a second human aflatoxin B_1-metabolising member of the aldo-keto reductase superfamily, AKR7A3, *Carcinogenesis 7*, 1215−1223.
14. Kelly, V., Ireland, L., Ellis, E., and Hayes, J. (2000) Purification from rat liver of a novel constitutively expressed member of the

aldo-keto reductase 7 family that is widely distributed in extrahepatic tissues, *Biochem. J. 348*, 389−400.

15. Hinshelwood, A., McGarvie, G., and Ellis, E. (2002) Characterisation of a novel mouse liver aldo-keto reductase AKR7A5, *FEBS Lett. 523*, 213−218.
16. Ellis, E. M., and Hayes, J. D. (1995) Substrate specificity of an aflatoxin-metabolizing aldehyde reductase, *Biochem. J. 312*, 535−541.
17. Hinshelwood, A., McGarvie, G., and Ellis, E. (2003) Substrate specificity of mouse aldo-keto reductase AKR7A5, *Chem.-Biol. Interact. 143−144*, 263−269.
18. Guengerich, F. P., Cai, H., McMahon, M., Hayes, J. D., Sutter, T. R., Groopman, J. D., Deng, Z., and Harris, T. M. (2001) Reduction of aflatoxin B1 dialdehyde by rat and human aldo-keto reductases, *Chem. Res. Toxicol. 14*, 727−737.
19. Schaller, M., Schaffhauser, M., Sans, N., and Wermuth, B. (1999) Cloning and expression of succinic semialdehyde reductase from human brain, *Eur. J. Biochem. 265*, 1056−1060.
20. Bradford, M. M. (1976) A rapid and sensitive method for the quantitation of microgram quantities of protein utilizing the principle of protein-dye binding, *Anal. Biochem. 72*, 248−254.
21. Otwinowski, Z., and Minor, W. (1997) Processing of X-ray diffraction data collected in oscillation mode, *Methods Enzymol. 276*, 307−326.
22. Collaborative Computational Project Number 4 (1994) The CCP4 suite: Programs for Protein Crystallography, *Acta Crystallogr. D50*, 760−763.
23. Navaza, J. (1994) AMoRe: An automated Package for Molecular Replacement, *Acta Crystallogr. A50*, 157−163.
24. Matthews, B. W. (1968) Solvent content of protein crystals, *J. Mol. Biol. 33*, 491−497.
25. Murshudov, G. N., Vagin, A. A., and Dodson, E. J. (1997) Refinement of macromolecular structures by the maximum-likelihood method, *Acta Crystallogr. D53*, 240−255.
26. Kavanagh, K. L., Klimacek, M., Nidetzky, B., and Wilson, D. K. (2002) The structure of apo and holo forms of xylose reductase, a dimeric aldo-keto reductase from *Candida tenuis*, *Biochemistry 41*, 8785−8795.
27. Nicholas, C. P., and Lewis, S. (1999) *Fundamentals of Enzymology: The Cell and Molecular Biology of Catalytic Proteins*, 3rd ed., Oxford University Press, Oxford, U.K.
28. Harrison, D. H., Bohren, K. M., Petsko, G. A., Ringe, D., and Gabbay, K. H. (1997) The alrestatin double-decker: Binding of two inhibitor molecules to human aldose reductase reveals a new specificity determinant, *Biochemistry 36*, 16134−16140.
29. Penning, T. M., Bennett, M. J., Smith-Hoog, S., Schlegel, B. P., Jez, J. M., and Lewis, M. (1997) Structure and function of 3α-hydroxysteroid dehydrogenase, *Steroids 62*, 101−111.
30. Wilson, D. K., Nakano, T., Petrash, J. M., and Quiocho, F. A. (1997) Structural studies of aldo-keto reductase inhibition, *Adv. Exp. Med. Biol. 414*, 435−442.

BI051610K